Mo-Doped CdS: Optimized Electronic Structure Boosts Carrier Separation.

Ning Zhang [a], Hui Zhao [b], Xiaoyu Liu [a], Jiyue Ding [a], Huachi Yu [b], Yan Liu [a], Qingyang Xu[a], Ke Cui [a], Yi Wang [a], Qian Zhang [a], Hailin Cong [a*]*

[a] School of Resources and Environmental Engineering, Shandong University of Technology, 255049 Zibo, PR China

[b] School of Agricultural Engineering and Food Science, Shandong University of Technology, 255049 Zibo, PR China

Corresponding author: Qian Zhang, zq@sdut.edu.cn

Hailin Cong, conghailin@sdut.edu.cn

Photocatalytic activity test

The solution was irradiated using a 180 $W \cdot m^{-2}$ xenon lamp emitting visible light ($\lambda > 420$ nm). A total of 10 mg of photocatalyst was dispersed in 30 mL of TC solution at a concentration of 20 mg/L. To establish an adsorption-desorption equilibrium, the mixture was stirred in the dark for 30 minutes. Subsequently, under visible light irradiation, 2 mL of the solution was filtered every 20 minutes for analysis of TC concentration via HPLC. The degradation stability of the photocatalyst was assessed through three consecutive cycles, with the experimental procedure for each cycle mirroring that of the photocatalytic degradation performance tests. After each cycle, the samples were thoroughly rinsed with deionized water and dried.

To investigate the active species involved in the reaction, a series of species capture experiments were conducted. Building upon the foundational tests of photocatalytic degradation performance, we selectively introduced 1 mM of EDTA-2Na, BQ, and IPA to capture holes (h^+), superoxide radicals ($\cdot O_2^-$), and hydroxyl radicals ($\cdot OH$), respectively. The subsequent experimental procedures adhered to the same protocol as the photocatalytic degradation performance tests. All experiments were replicated three times to ensure reliability and accuracy of the results.

Photochemical Testing

The photoelectrochemical testing was conducted utilizing a standard three-electrode system, wherein an Ag/AgCl electrode served as the reference electrode, a platinum wire acted as the counter electrode, and the sample FTO functioned as the working electrode. Under ambient air conditions, a 0.1 M Na_2SO_4 solution was employed as the electrolyte, with a 180 $W \cdot m^{-2}$ Xe lamp providing the light source. The preparation of the working electrode was executed as follows: 5 mg of the sample was dispersed in 500 μL of ethanol and subjected to ultrasonic treatment for 10 minutes. Following thorough dispersion, 200 μL of the resulting solution was pipetted onto a 1 cm × 1.5 cm FTO working electrode, which was subsequently dried at 60°C for 4 hours.

DFT Calculations

Plane-wave density functional theory (DFT) calculations were performed using the Material Studio software to model CdS and Mo-doped CdS. The generalized gradient approximation (GGA) with the Perdew-Burke-Ernzerhof (PBE) exchange-correlation functional and ultrasoft pseudopotentials were employed in the simulations. A 340eV cutoff energy was applied to the plane-wave basis set. A 3×3×1 supercell was adopted for the CdS materials. The lattice

parameters for Mo-CdS are a= b=16.504, c= 13.369 A, while in CdS, a=b=16.546, c=13.456.

This study utilized Gaussian 16 to optimize the structure of TC and predict the degradation sites of the pollutant. The concentrated Fukui functions were calculated using Multiwfn 3.8, and electrophilic and radical reaction sites were predicted based on Hirshfeld charge analysis. All calculations were performed with the IEFPCM solvent model at the B_3LYP/6-31+G** level.

Characterization and Testing

The X-ray diffraction (XRD) patterns are obtained using an X-ray diffraction D8 ADVANCE instrument with Cu Kα radiation in the 10-70 range. Fourier Transform Infrared (FT-IR) spectra were obtained using a Nicolet 5700 FTIR spectrophotometer over the range of 4000-500 cm-1 at a resolution of 2 cm-1. X-ray photoelectron spectroscopy (XPS) was conducted using the Thermo Scientific K-Alpha instrument. The concentration of TC in the solution was determined using the UltiMate 3000 HPLC system. The surface morphology and microstructure of the samples were characterized using a scanning electron microscope (SEM) model JSM6700F. Transmission electron microscopy (TEM) and high-resolution transmission electron microscopy (HR-TEM) images are acquired using a field emission high-resolution transmission electron microscope (JEOL JEM 2010) operating at a 200 kV accelerating voltage. Brunauer-Emmett-Teller (BET) specific surface area of solid samples and Pore size distributions are determined by N2 adsorption–desorption test (Edinburgh FLS1000). The morphology and surface potential are characterized using an Atomic Force Microscope (AFM) and Kelvin Probe Force Microscope (KPFM) on the Bruker Dimension ICON instrument. Photoluminescence (PL) spectra are measured using an FLS-980 fluorescence spectrometer. The decay curve of time-resolved photoluminescence (TR-PL) is recorded using an FLS920 fluorescence lifetime spectrophotometer. Electron paramagnetic resonance (EPR) spectra were taken using a Bruker model A300 emx-plus spectrometer.

The first-order dynamic model is as follows:

$$Eq.S1 \quad -Ln\left(\frac{C_t}{C_A}\right) = k_1 t$$

In this context, CA and C (mg/L) represent the concentrations of reactants at the initial time (0 minutes) and at time t (in minutes), respectively. The parameter k_1 denotes the pseudo-first-order rate constant, and t signifies the duration of the reaction. The regression curve of $-Ln(C_t/C_A)$ plotted against t exhibits linearity, from which the value of k_1 can be derived from the slope of the graph.

The second-order dynamical model is presented as follows:

$$Eq.S1 \quad \frac{t}{q_t} = \frac{1}{k_2 \times q_e^2} + \frac{1}{q_e} \times t$$

$$Eq.S1 \quad q_t = (C_A - C_t) \times \frac{V}{m}$$

In this context, q_e (mg/g) and q_t (g/mg) represent the amount of reactant degradation at equilibrium and at a given reaction time t, respectively. The constant rate k_2 ($mg \cdot g^{-1} \cdot min^{-1}$) corresponds to the pseudo-second-order reaction. V (mL) denotes the volume of the solution, while m (g) refers to the mass of the photocatalyst introduced into the solution. The regression curve of t/q_t against t is linear, allowing for the determination of q_e and k_2 from the slope and intercept of the graph, respectively.

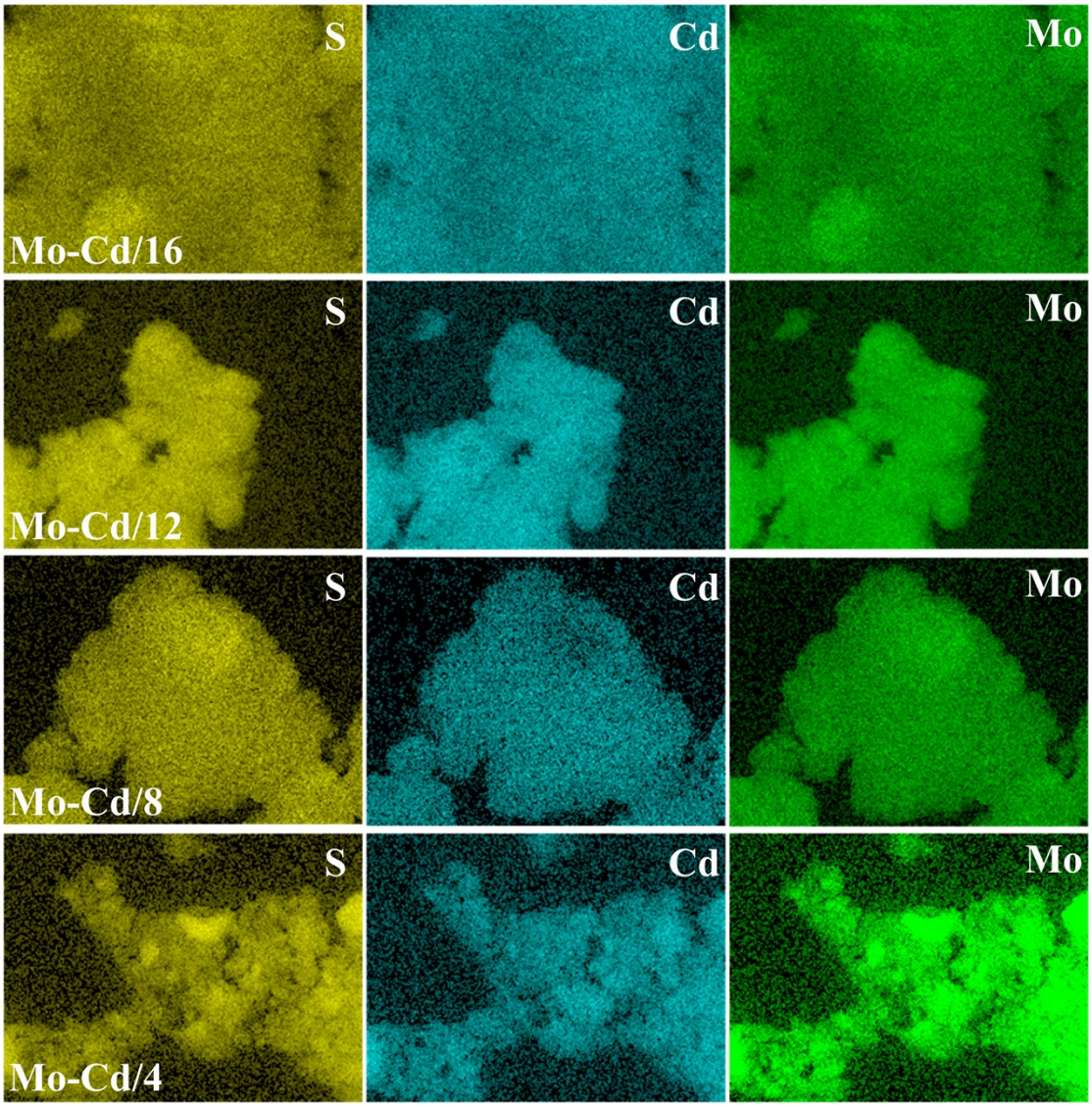

Fig. S1. EDX mapping of Mo-Cd/16, Mo-Cd/12, Mo-Cd/8, Mo-Cd/4.

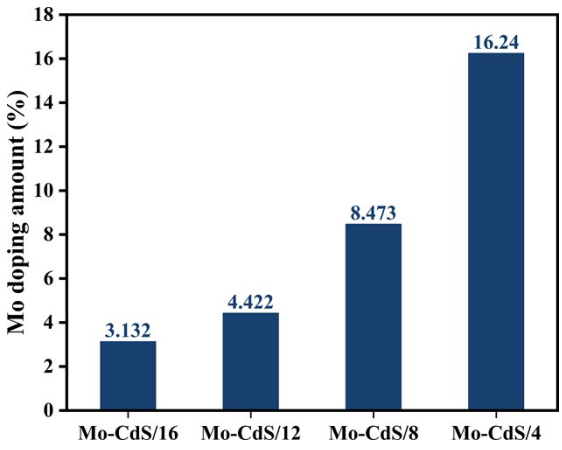

Fig. S2. The ICP measured the Mo content in the Mo-Cd/16, Mo-Cd/12, Mo-Cd/8, and Mo-Cd/4 samples.

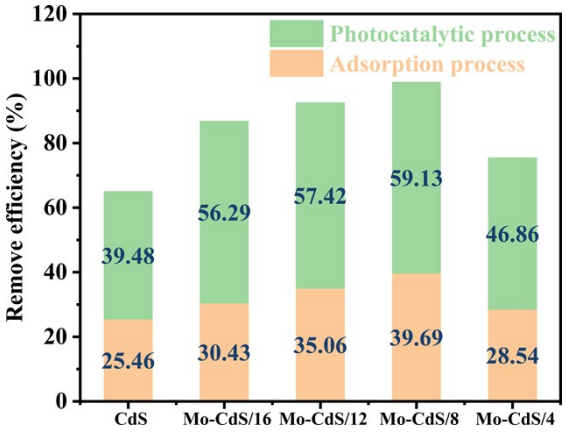

Fig. S3. TC removal efficiency.

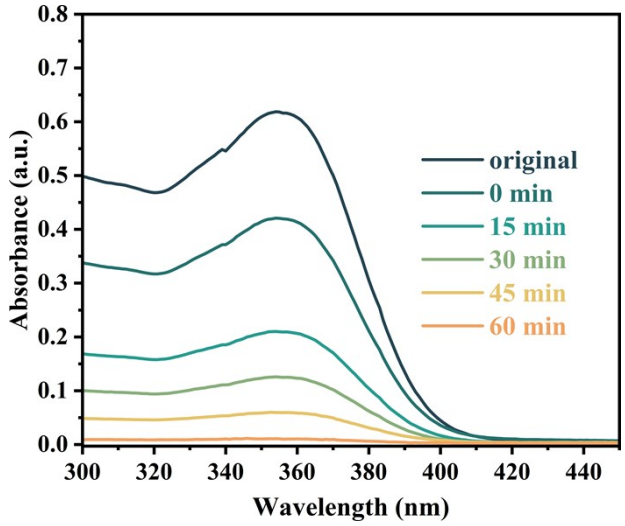

Fig. S4. The changes of TC absorption peak versus time.

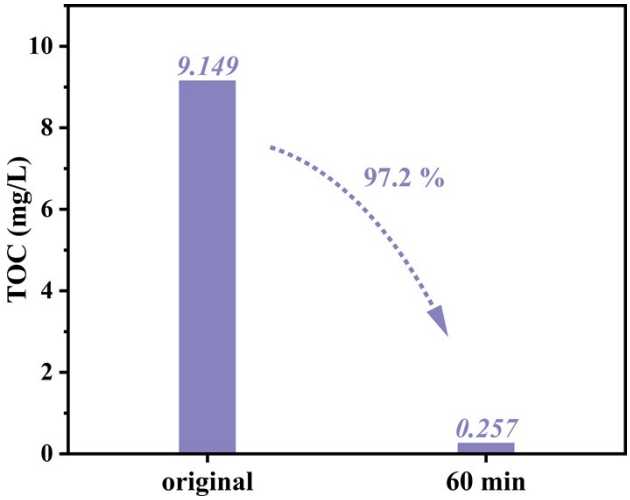

Fig. S5. TOC content after 60 minutes of reaction

Table S1. Kinetic Parameters for the Photocatalytic Degradation of Tetracycline

	Pseudo-first-order		Pseudo-second-order	
	k_1 (min^{-1})	R^2	k_2 (mg g^{-1} min^{-1})	R^2
CdS	0.0125	0.9698	0.0385	0.8442
Mo-CdS/16	0.0271	0.9607	0.0281	0.9472
Mo-CdS/12	0.0360	0.9360	0.0276	0.9704
Mo-CdS/8	0.0650	0.9526	0.0275	0.9931
Mo-CdS/4	0.0173	0.8961	0.0337	0.9523

Table S2. Comparison of different photocatalysts reported for TC degradation.

Reaction system	Initial tetracycline concentration (mg/L)	Catalyst dosage (g/L)	Time (min)	Degradation efficiency	Reference
TiO_2/MIL-101(Cr)	10	0.20	90	99.70%	[1]
S_3-MIL-53(Fe)	50	0.10	60	96.80%	[2]
MIL-88B@COF-200@10%PANI	50	0.33	120	97.40%	[3]
nNH_2-MIL-125(Ti)(TiO_2)/Ti_3C_2	10	0.05	60	82.00%	[4]
NH_2-MIL-125(Ti)/BiOCl	20	0.05	120	78.00%	[5]
2D Cu-TCPP MOFs	10	0.05	360	86.30%	[6]
$ZnIn_2S_4$@PCN-224	20	0.20	60	99.90%	[7]
Ag_3PO4/MIL-53(Fe)	20	0.50	60	93.70%	[8]
Zr-MOF@WO_3/graphene	20	1.70	70	84.00%	[9]
Mo-CdS/8	20	0.025	60	98.82%	**This work**

Table S3. Fluorescence Lifetime (τAVE) and Associated Parameters of Photocatalysts

Sample	τ_1 (nm)	τ_2 (nm)	B_1	B_2	τ_{AVE} (nm)
CdS	1.39	6.27	327.39	0.96	1.45
Mo-CdS/16	0.86	2.37	30.29	3837.46	2.36
Mo-CdS/12	0.91	2.39	22.39	4423.93	2.38
Mo-CdS/8	1.07	3.01	7.57	1583.41	3.01
Mo-CdS/4	0.80	2.3	36.17	4536.85	2.29

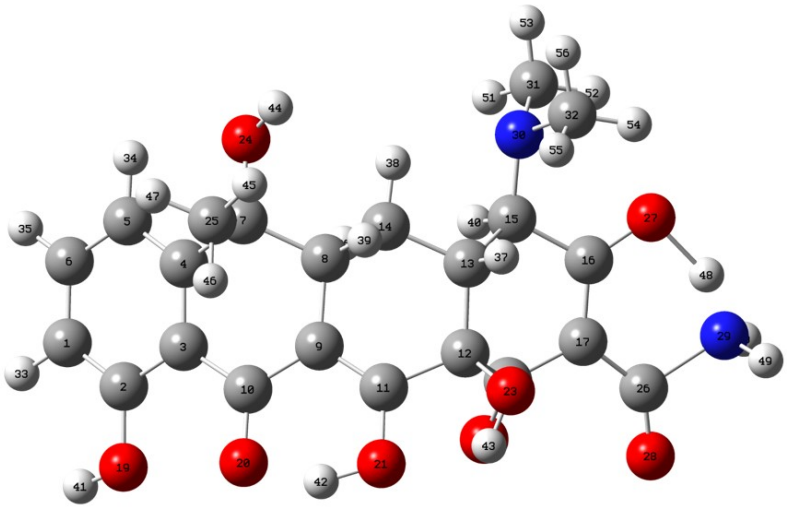

Fig. S6. Optimized chemical structure of CIP

Table S4. Molecular size model of degradation process

No.	Model	Dimensions (length, width and height)
P1	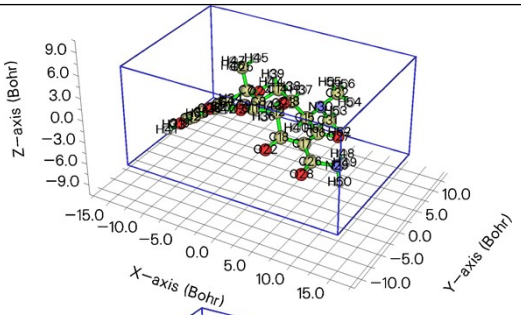	15.099, 10.290 and 7.223
P2	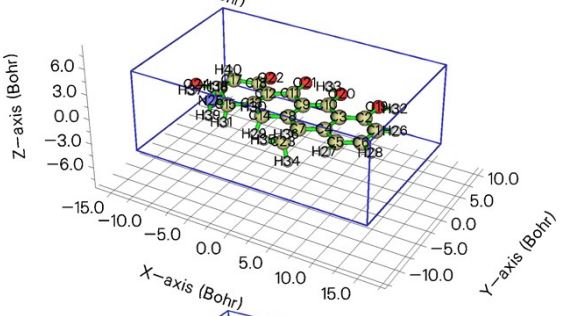	14.948, 9.402 and 5.225
P3	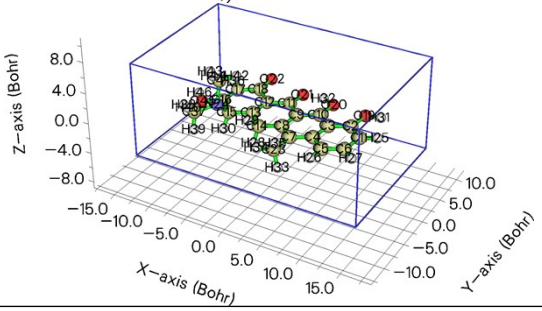	15.402, 9.809 and 6.566

P4	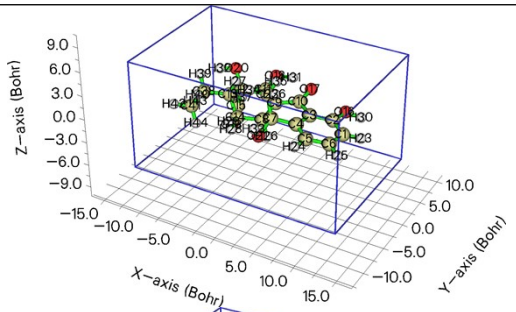	13.850, 9.005 and 7.364
P5	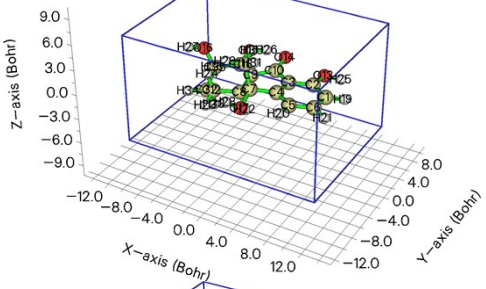	12.244, 8.859 and 6.977
P6	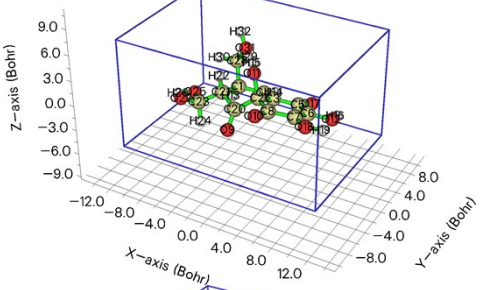	12.354, 8.495 and 6.929
P7	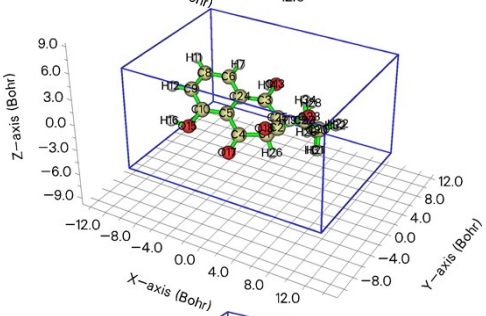	12.187, 8.900 and 6.473
P8	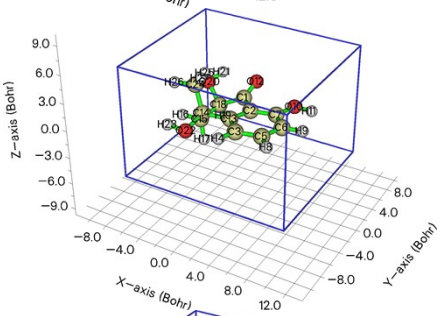	9.485, 8.318 and 76.594
P9	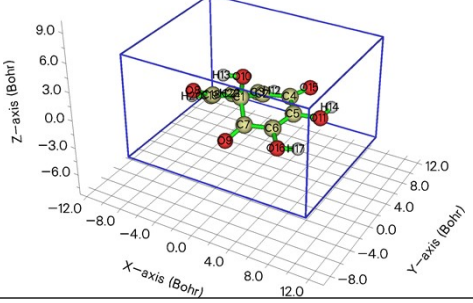	10.120, 8.026 and 5.896

P10	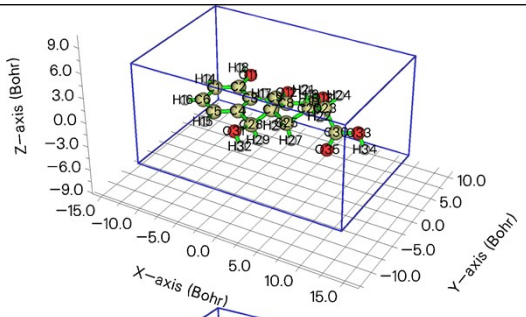	13.449, 8.834 and 6.742
P11	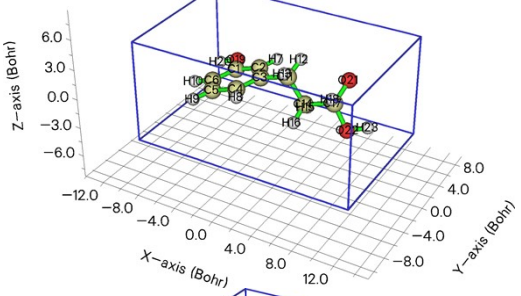	11.571, 7.299 and 5.436
P12	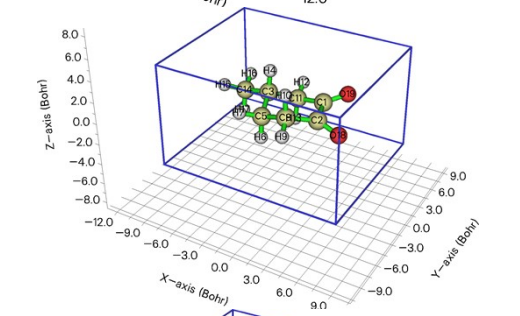	8.933, 7.147 and 5.251
P13	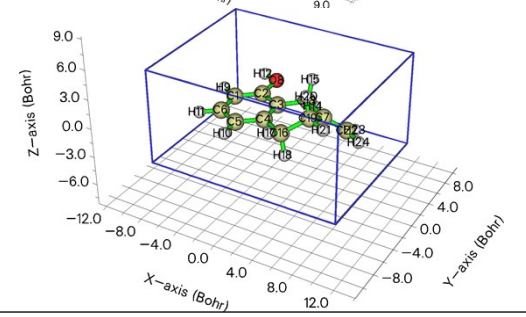	10.293, 8.000 and 5.278

Table S5. NPA charge distribution and Fukui index of TC

Number	Atom	q(N)	q(N+1)	q(N-1)	f^-	f^+	f^0
1	C	-0.0997	-0.0466	0.0257	0.0273	0.0265	0.0016
2	C	0.0668	0.1177	0.0271	0.0238	0.0254	-0.0033
3	C	-0.0388	-0.0091	0.0199	0.0098	0.0148	-0.0101
4	C	-0.0124	0.0166	0.0057	0.0233	0.0145	0.0177
5	C	-0.0738	-0.0167	0.0357	0.0214	0.0285	-0.0143
6	C	-0.0783	0.0037	0.0303	0.0518	0.041	0.0215
7	C	0.095	0.0967	0.0008	0.001	0.0009	0.0002
8	C	-0.0293	-0.023	0.0042	0.0021	0.0031	-0.0021
9	C	-0.0807	-0.0251	0.0406	0.015	0.0278	-0.0255

10	C	0.0627	0.1348	0.0076	0.0645	0.036	0.0568
11	C	0.0507	0.1187	0.0226	0.0454	0.034	0.0228
12	C	0.07	0.0792	0.0022	0.007	0.0046	0.0047
13	C	-0.0159	-0.0102	0.0033	0.0024	0.0028	-0.0009
14	C	-0.0598	-0.051	0.0042	0.0046	0.0044	0.0005
15	C	0.0283	0.0404	0.0079	0.0042	0.006	-0.0038
16	C	0.0584	0.1073	0.0009	0.0481	0.0245	0.0472
17	C	-0.0926	-0.0593	0.0169	0.0164	0.0166	-0.0005
18	C	0.1027	0.1323	0.0023	0.0273	0.0148	0.025
19	O	-0.2006	-0.1377	0.0453	0.0175	0.0314	-0.0278
20	O	-0.3123	-0.2112	0.0264	0.0746	0.0505	0.0482
21	O	-0.22	-0.1321	0.0457	0.0421	0.0439	-0.0036
22	O	-0.2866	-0.2191	0.023	0.0444	0.0337	0.0214
23	O	-0.2626	-0.2207	0.015	0.0268	0.0209	0.0117
24	O	-0.2437	-0.2234	0.0089	0.0114	0.0101	0.0025
25	C	-0.0997	-0.0892	0.0046	0.006	0.0053	0.0014
26	C	0.156	0.1776	0.006	0.0155	0.0108	0.0095
27	O	-0.2062	-0.1683	0.0019	0.036	0.019	0.0341
28	O	-0.305	-0.2408	0.0286	0.0355	0.0321	0.007
29	N	-0.1603	-0.1367	0.0093	0.0143	0.0118	0.0051
30	N	-0.097	0.0246	0.1209	0.0007	0.0608	-0.1202
31	C	-0.0449	-0.0158	0.0248	0.0043	0.0145	-0.0205
32	C	-0.0455	-0.0171	0.0242	0.0041	0.0142	-0.0201
33	H	0.022	0.0611	0.0183	0.0207	0.0195	0.0024
34	H	0.0276	0.0594	0.0157	0.0161	0.0159	0.0004
35	H	0.0243	0.0701	0.0193	0.0265	0.0229	0.0072
36	H	0.0189	0.0363	0.0094	0.0081	0.0087	-0.0013
37	H	0.0283	0.0459	0.0072	0.0104	0.0088	0.0031
38	H	0.012	0.0279	0.0041	0.0118	0.0079	0.0077
39	H	0.0225	0.0412	0.011	0.0077	0.0093	-0.0033
40	H	0.0313	0.0492	0.008	0.01	0.009	0.002
41	H	0.1652	0.2042	0.0207	0.0182	0.0195	-0.0025
42	H	0.1311	0.1574	0.012	0.0143	0.0132	0.0024
43	H	0.1495	0.171	0.0101	0.0113	0.0107	0.0012
44	H	0.1488	0.1653	0.0055	0.011	0.0082	0.0055

45	H	0.0197	0.038	0.0068	0.0115	0.0092	0.0047
46	H	0.0362	0.0414	0.0034	0.0018	0.0026	-0.0016
47	H	0.0249	0.0474	0.0108	0.0117	0.0112	0.0009
48	H	0.1332	0.1558	0.0095	0.0131	0.0113	0.0035
49	H	0.1192	0.1479	0.0122	0.0165	0.0144	0.0043
50	H	0.1251	0.1383	0.0047	0.0085	0.0066	0.0038
51	H	0.0321	0.0537	0.0195	0.0022	0.0108	-0.0173
52	H	0.0117	0.0592	0.0402	0.0073	0.0237	-0.0328
53	H	0.0219	0.0588	0.0254	0.0114	0.0184	-0.014
54	H	0.012	0.0576	0.0387	0.0069	0.0228	-0.0319
55	H	0.0366	0.0571	0.0187	0.0018	0.0103	-0.0169
56	H	0.0212	0.0597	0.0263	0.0122	0.0193	-0.014

References

[1] J. Chen, X. Zhang, X. Shi, F. Bi, Y. Yang, Y. Wang, Synergistic effects of octahedral TiO_2-MIL-101(Cr) with two heterojunctions for enhancing visible-light photocatalytic degradation of liquid tetracycline and gaseous toluene, J. Colloid. Interface Sci., 579 (2020) 37-49. https://doi.org/10.1016/j.jcis.2020.06.042.

[2] H. Chen, X. Yuan, L. Jiang, H. Wang, H. Yu, X. Wang, Intramolecular modulation of iron-based metal organic framework with energy level adjusting for efficient photocatalytic activity, Appl. Catal. B: Environmental, 302 (2022). https://doi.org/10.1016/j.apcatb.2021.120823.

[3] S.-W. Lv, J.-M. Liu, F.-E. Yang, C.-Y. Li, S. Wang, A novel photocatalytic platform based on the newly-constructed ternary composites with a double p-n heterojunction for contaminants degradation and bacteria inactivation, Chem. Eng. J., 409 (2021). https://doi.org/10.1016/j.cej.2020.128269.

[4] Y. Wu, X. Li, Q. Yang, D. Wang, F. Yao, J. Cao, Z. Chen, X. Huang, Y. Yang, X. Li, Mxene-modulated dual-heterojunction generation on a metal-organic framework (MOF) via surface constitution reconstruction for enhanced photocatalytic activity, Chem. Eng. J., 390 (2020). https://doi.org/10.1016/j.cej.2020.124519.

[5] Q. Hu, J. Di, B. Wang, M. Ji, Y. Chen, J. Xia, H. Li, Y. Zhao, In-situ preparation of NH_2-MIL-125(Ti)/BiOCl composite with accelerating charge carriers for boosting visible light photocatalytic activity, Appl. Surface Sci., 466 (2019) 525-534. https://doi.org/10.1016/j.apsusc.2018.10.020.

[6] S. Zhao, S. Li, Z. Zhao, Y. Su, Y. Long, Z. Zheng, D. Cui, Y. Liu, C. Wang, X. Zhang, Z. Zhang, Microwave-assisted hydrothermal assembly of 2D copper-porphyrin metal-organic frameworks for the removal of dyes and antibiotics from water, Environ. Sci. Pollut. Res. Int., 27 (2020) 39186-39197. https://doi.org/10.1007/s11356-020-09865-z.

[7] P. Jin, L. Wang, X. Ma, R. Lian, J. Huang, H. She, M. Zhang, Q. Wang, Construction of hierarchical ZnIn2S4@PCN-224 heterojunction for boosting photocatalytic performance in hydrogen production and degradation of tetracycline hydrochloride, Appl. Catal. B, 284 (2021). https://doi.org/10.1016/j.apcatb.2020.119762.

[8] L. Xie, Z. Yang, W. Xiong, Y. Zhou, J. Cao, Y. Peng, X. Li, C. Zhou, R. Xu, Y. Zhang, Construction of MIL-53(Fe) metal-organic framework modified by silver phosphate nanoparticles as a novel Z-scheme photocatalyst: Visible-light photocatalytic performance and mechanism investigation, Appl. Surface Sci., 465 (2019) 103-115. https://doi.org/10.1016/j.apsusc.2018.09.144.
[9] H. Fakhri, H. Bagheri, Highly efficient Zr-MOF@WO_3/graphene oxide photocatalyst: Synthesis, characterization and photodegradation of tetracycline and malathion, Materials Science in Semiconductor Processing, 107 (2020). https://doi.org/10.1016/j.mssp.2019.104815.